Journal of Sustainability Science and Management
Volume 18 Number 12, December 2023: 66-83
eISSN: 2672-7226

GROUNDWATER POTENTIAL (GWP) ZONE MAPPING USING THE INTEGRATION OF REMOTE SENSING AND GEOGRAPHIC INFORMATION SYSTEM (GIS), CASE STUDY: HULU LANGAT, SELANGOR

SHARIFAH NORASHIKIN BOHARI[1]*, ABDULLAH AIMAN AZIZ[2], ROHAYU HARUN NARASYID[1,2], NURSYAHANI NASRON AND SUHAILA HASHIM[1]

[1]Climate Change and Environmental Research Group Centre of Studies for Surveying Science and Geomatics, Faculty of Architecture, Planning and Surveying, Universiti Teknologi MARA, Perlis Branch, Arau Campus, 02600 Arau, Perlis, Malaysia. [2]Centre of Studies for Surveying Science and Geomatics, Faculty of Architecture, Planning and Surveying, Universiti Teknologi MARA, Perlis Branch, Arau Campus, 02600 Arau, Perlis, Malaysia.

**Corresponding author: ashikin10@uitm.edu.my*
Submitted final draft: 4 January 2023 *Accepted: 7 March 2023* http://doi.org/10.46754/jssm.2023.12.007

Abstract: Assessing potential sources related to water scarcity management faces difficulties in terms of time and expenses, particularly in sustaining groundwater systems and efficient water distribution. The purpose of this study is to assess the capabilities of remote sensing images in extracting soil moisture content for groundwater potential (GWP) identification using Sentinel 1A and Landsat 8 images. Ten (10) conditional parameters (slope, curvature, drainage density, lineament density, elevation, geology map, rainfall, land used land cover (LULC), soil moisture, and geomorphology; and twenty-two (22) tube wells have been used to identify the GWP area. In ArcGIS software, the Analytical Hierarchy Process (AHP) approach has been utilised to assign the weightage of thematic layer parameters and overlay weight in spatial analysis. Two (2) GWP areas have been generated and are assessed utilising existing tube well distribution. An agreement between expected and actual for both GWP maps is obtained with an accuracy of 85.71%. The findings of regression of groundwater validation for Sentinel 1A and Landsat 8 show the coefficient of association of ($r = 0.983$) and ($r = 0.372$), respectively. The study's findings aid planners, politicians, and local governments by providing first-hand knowledge for future planning initiatives to guarantee the sustainable use of groundwater resources.

Keywords: Groundwater Potential Area (GWPA), AHP, soil moisture.

Introduction

Water is the most vital and valuable resource for human life. Therefore, sustaining a clean water supply has long been prominent in the national and international agendas. Poor basin management for surface water resources and long drought periods are the global issues that contribute to the water shortage. Thus, groundwater is an alternative natural resource that plays a vital role in ensuring the health of urban and rural residents, fostering sustainable economic and social growth, and preserving the ecological balance. The demand/requirement for groundwater has grown tremendously due to population growth, advanced irrigation methods, and industrial uses. Thus, water supply management and sustainability of groundwater resources must be considered to detect the potential groundwater sources, thus ensuring continuous water supply. Furthermore, major cities in Malaysia are experiencing challenges in supplying potable water due to population growth, rapid industrialisation, surface water pollution, and drought factors. The groundwater level has dropped by 0.5-3 metres in most districts in Selangor, including Klang, Langat, and Bernam basins due to extreme heat. The groundwater level is also expected to drop by 0-1 metre due to changes in land use (Mridha *et al.*, 2020).

Conventionally, the hydrological test is required for groundwater identification processes, which involve extensive drilling, ground surveys, and geophysical technologies (Serele *et al*., 2020). These approaches are

expensive, time-consuming, and labour-intensive. Nowadays, the potential location of groundwater resources can be detected by using geospatial approaches. The example of the sophisticated approaches in geospatial technology are Unmanned Aerial Vehicle (UAV) mapping (Zamari *et al.,* 2019) and Ground Penetrating Radar (GPR) System (Elsheakh & Abdallah, 2019) and Remote Sensing technology (Sibanda *et al.,* 2015). Currently, Remote Sensing technologies with the integration of Geographic Information Systems (GIS) have been widely employed in groundwater detection over the last few decades (Singh *et al.*, 2019). Several researchers (Jenifer & Jha, 2017; Misi *et al.*, 2018; Ifediegwu, 2022; Sajil Kumar *et al*., 2022) use the Integrated Remote Sensing (RS) approach, GIS, and Multi-Criteria Decision Analysis (MCDA) techniques to identify potential groundwater areas and uncover suitable artificial recharging sites. They discovered that MCDA is an effective method to determine the GWP areas (Misi *et al.,* 2018; Osinowo & Arowoogun, 2020).

Based on the hydrological and geological features, the groundwater parameters can be classified into direct and indirect indicators. Rainfall is the most dominant factor for an area's groundwater potential, as it is the primary source of water in the hydrological cycle (Ibrahim-Bathis & Ahmed, 2016a). In addition to rainfall, groundwater occurrence and movement depend on the geological setting (Jhariya *et al.,* 2016). As reviewed by Nigussie *et al.* (2019), the primary indicator, i.e. hydrological features are related to the establishment of groundwater such as recharge and discharge zones, soil moisture, and vegetation. The secondary indicators, i.e. geological features are associated with rock and soil type, structures including fracture zones, landforms, and drainage characteristics. Delineation of groundwater using spatial data involves multiple attribute decision-making which requires a group of parameters that are appraised on the core of competitive and disproportionate criteria (Malczewski, 1999). Several parameters must be considered, including soil moisture, soil texture, geological unit (Nigussie *et al.*, 2019), soil drainage, slope, lithology and aspects (Singh *et al*., 2019), slope, topography, stream network and lithology (Mokadem *et al*., 2018), and drainage systems, rainfall, altitude (Misi *et al.,* 2018) which play a crucial role. Díaz-Alcaide and Martínez-Santos (2019) reveal a group of parameters which consistently utilised by many researchers including lithology (geology), geomorphology, soil, land use/land cover, topography, lineaments, drainage and slope-related variables, rainfall and groundwater recharge.

However, research from previous studies used various types of either optical or microwave sensors in extracting soil moisture parameters, including Sentinel images (Sutariya *et al*., 2021), Landsat 8 (Naghibi *et al.,* 2017; Chen *et al*., 2018; Wang *et al.*, 2021), MODIS (Parks *et al*., 2017; Abrams *et al.*, 2018) and from in-situ method (Sharma *et al*., 2018; Sutariya *et al.*, 2021). Entezari *et al*. (2019) has reported that the coefficient of determination of soil moisture content using Landsat 8 image is 0.959, while Sutariya *et al*. (2021) has achieved the coefficient of determination for similar parameter from Sentinel 1A image up to 0.788. Thus, the purpose of this research is to investigate the capability of various sensors from microwave and optical remote sensing images in extracting soil moisture content for GWP areas in Hulu Langat. Sentinel 1A and Landsat 8 images are employed in this study to extract soil moisture. Ten (10) conditioning factors have also been included in determining GWP areas over the study region.

Materials and Methods

This research is divided into five (5) phases: (1) study area and software selection; (2) data acquisition; (3) soil moisture estimation using Sentinel 1A and Landsat 8, (4) GWP area determination; and (5) data validation. In Phase 1, Hulu Langat is selected as the study area, and SNAP and ArcMap 10.5 software are used in this research for soil moisture extraction and the GWP area determination process. Phase 2 involves a data acquisition process for preparing

the thematic data layers including Sentinel 1A, Landsat 8, TanDEM-X, geological map, rainfall data and tube wells distribution. Phase 3 focuses on data processing and extraction of conditioning parameters layers. Soil moisture content is extracted from Sentinel 1A and Landsat 8 satellite images. Thematic layers, such as curvature, slope, elevation, drainage density, lineament density, and geomorphology are derived from DEM data with 30m resolution. Finally, geological units are derived from geological maps through the digitisation process, and mean monthly rainfall is interpolated from rainfall station data. In Phase 4, two (2) GWP areas are developed from both sensors using the APH approach by determining the weightage for every thematic layer. In Phase 5, the results are validated using tube well data. Figure 1 shows the summary of the research methodology implemented in the study.

Conditioning Parameters Preparation

Delineation of GWP areas involves ten (10) different conditioning parameters retrieved from several sources. Soil moisture content is retrieved from Sentinel 1A and Landsat 8; slope, geomorphology, drainage density, lineament density, elevation, and curvature are derived from TanDEM-X data; geological units are derived from geological maps; rainfall data are interpolated from rainfall station data; and LULC is derived from Landsat 8.

Soil motion estimation: Soil moisture estimation from both optical and microwave images is processed from Sentinel 1A and Landsat 8 images. Sentinel 1A images for February, April, and June 2021 with a spatial resolution of 10m are retrieved from the Copernicus scientific data hub and the images are utilised for soil moisture extraction. Pre-processing procedure which involves:

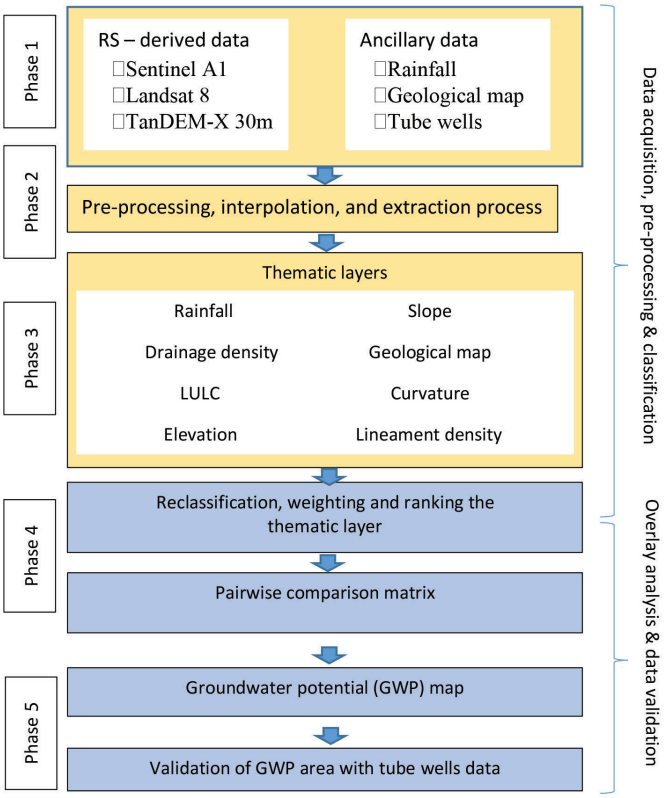

Figure 1: Research methodology workflow

(1) applying orbit file to satellite images; (2) removing thermal and border noise; (3) performing radiometric calibration, multi-looking, and terrain correction; and (4) converting to dB in Sentinel Application Platform software (SNAP). Three (3) images retrieved from Landsat 8 satellite from February, April, and June 2021 are downloaded from the USGS website and utilised in the soil moisture extraction process using ArcGIS software. All the equations derived using ArcMap's raster calculator and Land Surface Temperature (LST) are determined using band 10 TIRS and band 4 with 5 OLI. The Landsat 8 (bands 4 and 5) image processing is included to determine the NDVI proportion of vegetation and land surface emissivity, while band 10 TIRS data are used to determine brightness temperature before all of the bands are combined to retrieve the LST in the study area.

Slope: Slope is the rate of elevation changes, and it is also a key element in determining groundwater potential zones. High runoff and surface soil erosion are caused by increased slopes (Ibrahim-Bathis & Ahmed, 2016). Slopes are generated from 30m DEM resolution by creating surfaces from the surface analyst tool in ArcGIS. The slope of the groundwater potential map has been reclassified into five categories, which are 0-2, 2-5, 5-10, 10-30, and >30 degrees based on the slope elevation.

Drainage Density: Drainage density has been calculated from the retrieved DEM by dividing the entire length of the stream by its contribution area. The line density tool included in the ArcGIS toolbox is used to map the drainage density in Hulu Langat. Firstly, Fill is created from DEM data, and it is utilised to construct flow direction. Then, flow accumulation is created, followed by stream order. The streams are then converted into Features to create line density.

Lineaments Density: Lineaments are extracted from a 10m SAR image, and hill shade n-screen digitising is performed in ArcGIS using 30m DEM data. The process of creating lineament density is divided into three main stages. The initial step is to create a hill shadow for four (4) azimuths at altitudes of 315-45, 200-50, 100-60, and 50-90 degrees. A new polyline shapefile for lineament is then constructed before being categorised into five classes and classified according to their suitability for possible groundwater accumulation which are 0-0.26, 0.26 -0.68, 0.68-1.01,1.01-1.40 and 1.40-1.84.

Elevation: The elevation of the topographic surface generated from DEM is classified into five (5) classes (Adeyeye *et al.*, 2019).

Curvature: The curvature of the topographic surface generated from DEM with 30m resolution by generating curvature function in spatial analyst tool. The curvature is then classified into five (5) classes (Nair *et al*., 2017).

Rainfall: Monthly average rainfall data from three nearby stations are utilised to interpolate rainfall from February to June 2021. The rainfall map in ArcGIS is created using the Inverse Distance Weightage (IDW) interpolation technique (Ibrahim-Bathis & Ahmed, 2016). Before constructing climatic stations, the mean of rainfall data is determined, and then, it is imported and overlaid with the Hulu Langat shapefile.

Geomorphology: The geomorphology unit is derived from a high-resolution DEM. In ArcGIS, a hill shade is generated, and then slopes with (°) units are created. In this process, slopes are divided into five (5) classes. Landform features, slope, and aerial extent are utilised to map five (5) geomorphological units: smooth plain (SP), irregular plain (IP), escarpment, hills, and mountains (MHE), which are evaluated according to the appropriate rank of groundwater existence.

Geology: Geology maps of the research area are manually digitised. Starting with a georeferenced process where the coordinate of the geology map is defined. This map is classified into five (5) classes, including acid intrusive, Devonian, extrusive rocks, Permian, and vein quartz.

Land Used Land Cover (LULC): LULC is extracted from Landsat 8 data using supervised classification (Nigussie *et al.*, 2019). In this process, bands 1, 2, 3, 4, 5, 8, and 9 are utilised, stacked, select sampling area, and perform classification. Each class is then labelled based on the feature categories.

Reclassification Process

Each conditioning parameter has various effects on the occurrence of the GWP area. Different parameters are allocated to thematic layers, which are then converted to raster data format using the corresponding attribute. In order to satisfy the site-specific prerequisites for the AHP analysis, all the transformed layers are subjected to reclassification and resampling to ensure a consistent cell size of 10 m. Subsequently, the simplified raster data analysis is reclassified, wherein the range of cell values is categorised into a singular value based on the same rating approach (Nigussie *et al*., 2019). It is conducted to compare and assess the most and least appropriate locations. All the conditioning parameters and weights are inserted into a weighted overlay ArcGIS with a 1 to 5 evaluation scale as tabulated in Table 1.

Analytic hierarchy process (AHP) and Weighted Linear Combination (WLC)

MCDA approach is used in this study to identify the groundwater potential zones (Waikar & Nilawar, 2014). The rates for the classes as well as the weights and ranks for thematic layers, are computed using GIS-based multi-criteria evaluation based on Saaty's (1990) Analytical Hierarchy Process (AHP). As the potential impacts of each thematic layer of the model

Table 1: Reclassification and rating of layer suitability for groundwater potential zone

Thematic Layer	Description	Reclassification Values and Suitability Values for Groundwater Potential Zone Identification				
	Ranking	1	2	3	4	5
	Classification	Very Poor	Poor	Moderate	Good	Very Good
Geomorphology	Landform Types	Denudational hill	Denudational hill		Flood plain	Flood plain
Slope	Value in Degree	>30 (Very Steep)	10-30 (Steep)	5-10 (Moderate)	2-5 (Gentle)	0-2 (Level)
Geological Units	Types of Geological Units	Acid Intrusive	Phyllite and schist	Schist	Schist, phyllite, limestone	Schist, phyllite, limestone
Drainage Density	Value (Km/Km²) Category	0.0012-0.0061	0.0061-0.011	0.011-0.0159	0.0159-0.021	>0.0.026
Lineament Density	Density (Km/Km²)	<0.027	0.027- 0.54	0.54-0.81	0.81-1.08	1.08-1.35
LU/LC	Type	Bare land	Urban	Agriculture	Forest	Water Body
Rainfall	Value (mm)	2,750-3,000	2,500-2,750	2,250-2,500	2,000-2,250	
Elevation	Value (m)	-41.14 – 142.15	142.16 – 314.33	314.34 – 525.39	525.4 – 808.66	>808.67
Curvature	Value (m)	-0.71 – -0.211	-0.210 – -0.067	-0.066 – 0.060	0.061 – 0.234	0.235 – 0.76
Soil Moisture	Class (dB)		< -49& > -22	-22 to -18	-18 to 18	

aquifer recharge in different ways, weighting is used to consider the relative importance of each element. In this process, the weightage of all thematic layers is derived from a pairwise comparison reciprocal matrix of judgement. Then, the GWP map is generated using the weightage overlay method in ArcGIS software to identify the GWP area.

Data Validation

In order to determine the accuracy of the groundwater potential area, data such as borehole yield, hand-dug wells, and springs are overlayed with the groundwater potential area map (Hussein *et al.,* 2017; Nigussie *et al.,* 2019). For this study, the distribution of tube wells extracted from the hydrological map is used for data validation. In this process, the total amount of validation and disagreement data and the accuracy of the identified prospective zones are calculated (Nigussie *et al*., 2019) using the following equation.

$$GWPA = \left[\frac{Total\ Validation - Total\ Disagreement\ Data}{Total\ Validation\ Data}\right] \text{x } 100 \quad (1)$$

The most effective soil moisture content was acquired by computing the correlation coefficient in Excel from both maps generated by the different soil moisture content sensors.

Results and Discussion

Soil Moisture Content Extraction from Sentinel 1A dan Landsat 8 images

The backscattering coefficient radar (dB) is derived from Sentinel 1A satellite data. The decibel values obtained from the processing ranged from -39.79 to 33.76. They are then divided evenly into five (5) groups indicating the condition of soil moisture content: Very dry, dry, moderate, wet, and very wet. As represented in Figure 2 (a), the soil moisture content from very dry to very wet covers 44 km^2 (5%), 185 km^2 (22%), 303 km^2 (36%), 241 km^2 (29%), and 63 km^2 (8%) of the research area, respectively. Most of the dry and very dry areas are found in urban and developed areas, whereas moderate, wet, and very wet conditions are primarily covered by vegetation and water bodies. Soil moisture (SMI) extracted from Landsat 8 satellite images ranged from 9.62926e-007 to 1, representing from dry to wet. SMI values close to zero indicate water scarcity and low soil moisture content, while values close to one indicate a wet area or forest cover with the maximum moisture content (Tajudin *et al*., 2021).

Soil moisture (SMI) extracted from Landsat 8 satellite images ranged from 9.62926e-007 to 1, representing from dry to wet. SMI values close to zero indicate water scarcity and low soil moisture content, while values close to one indicate a wet area or forest cover with the maximum moisture content (Tajudin *et al.*, 2021). SMI content for Landsat 8 is also divided into five wetness levels: very dry, dry, moderate, wet, and very wet, as indicated in Figure 2 (b). Green areas represent very dry areas, which cover 3 km^2 or about 0.4% of the research area, whereas dark blue areas represent very wet areas, encompassing almost 4% or 31 km^2 in terms of area in the study region. Most of the dry and extremely dry areas are located in urban, bare land, and building areas, while wet areas are almost entirely covered by vegetation and water bodies, which indicates that 429 km^2 represents almost 51% of the study region.

SMI derived from Sentinel 1A image showed that the greatest indication was a moderate area, covering 303 km^2, or about 36% of the research area, while the lowest was very dry at just 5%, covering 44 km^2. While the greatest indication was wet, covering 429 km^2 and the lowest was extremely dry covering 31 km^{2,} representing 4% of Landsat 8 image extraction. According to Table 2, SMI extraction from both sensors demonstrates that Landsat 8 has better area coverage of good GWP region than Sentinel 1A. This is owing to the fact that excellent prospective groundwater area occurrence covered 51% of the area covered with a total of 429 km^2, and it covered largely in the northeast of the research region, which contains the majority of the vegetation area. Sentinel A1 covers just 241 km^2 for a respectable GWP area.

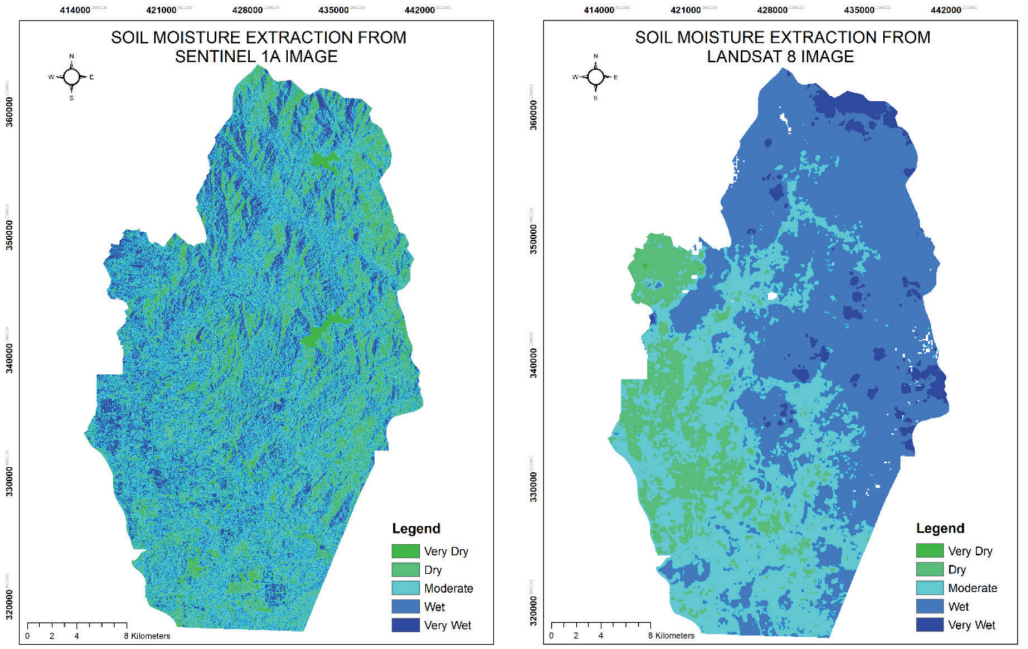

Figure 2: (a) Soil moisture from Sentinel 1A and (b) soil moisture from Landsat 8

Table 2: The SMI area retrieved from Sentinel 1A and Landsat 8 image

Image/Indication	Sentinel 1A		Landsat 8	
	Area (km^2)	Percentage (%)	Area (km^2)	Percentage (%)
Very Dry	44	5	3	0.4
Dry	185	22	100	12
Moderate	303	36	273	32.6
Wet	241	29	429	51
Very Wet	63	8	31	4

Geomorphology

The geomorphology map of Hulu Langat derived from DEM data shows different categories of landform conditions. The geomorphological are mapped based on five (5) characteristics: Irregular plain (IP), smooth plain (SP), escarpment, hills, and mountains. Figure 3 (a) depicts that most of the study areas are smooth plains and escarpments, which are shown in blue and green areas. Figure 3 (b) depicts the geomorphology maps that have been reclassified into three (3) criteria: Mountain, hill, and escarpment (MHE), smooth plain (SP), and irregular plain (IP), which are graded according to the present of groundwater. According to the classified image, MHE landforms cover almost 45% with covered for 361 km^2 of the study area. The SP covers 326 km^2, which represents about 41% of the area, while the IP comprises 14% of the area. Based on the geomorphology area, the high potential of the GWP area is identified as the largest area covered by SP (Hussein *et al.,* 2017).

Geology

Figure 4 shows six geological types: Acid intrusive, acid to intermediate, limestone/ marble, schist, and schist phyllite slate and limestone extracted from a geological map.

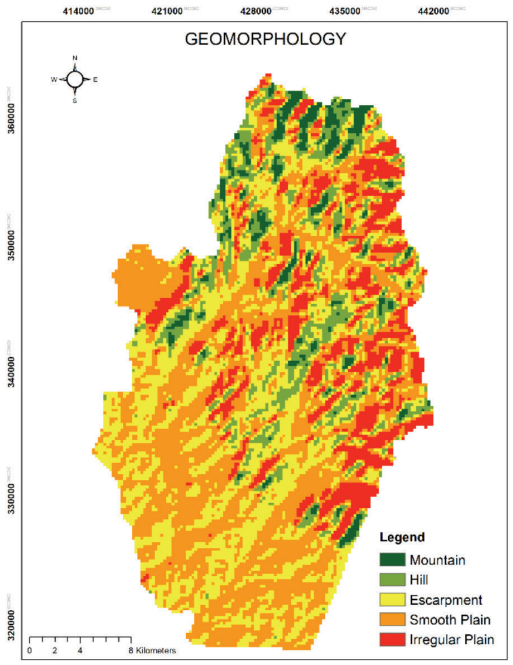

Figure 3: (a) Geomorphology

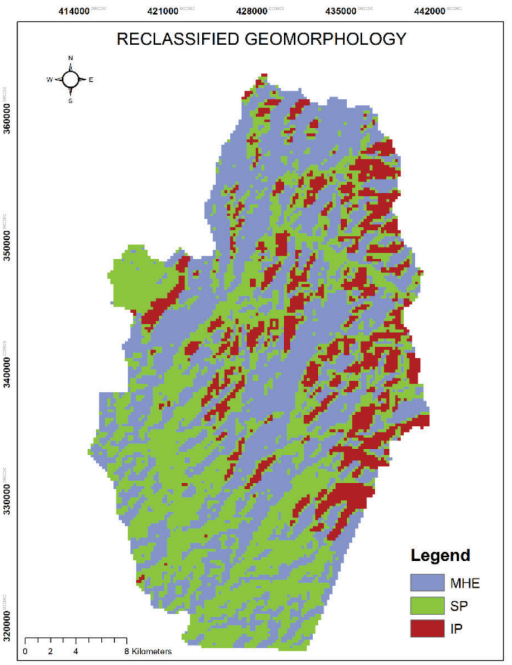

(b) Reclassified geomorphology

Figure 4 (a) indicates that 75% of the area, representing about 624 km^2 of the total study area, is covered with instructional acid. This kind of rock type may be challenging to work with due to its compact structure and lack of primary porosity (Dar *et al.,* 2021), both of which have an impact on the circulation of groundwater, which has the potential to result in a low potential for groundwater (Thakur & Raghuwanshi, 2008). The geological units that contain schist and phyllite, limestone, and sandstone cover almost 35% of the study area at 212 km^2, considered to have high-potential zones for groundwater, the reclassified geology map scale into rank 1 to 5.

Slope

The slope of the study area is retrieved from the DEM in degree units and the slope angles are divided into five (5) classes: 0°–2° (flat), 2°–5° (nearly flat), 5°–10° (mild), 10°–30° (moderate/ steep), and > 30°. (steep) as depicted in Figure 5. It is discovered that the study region is almost entirely covered by flat area, particularly in the southern region, where the slope degree ranges between 0°–2° and 2°–5°. This indicates high GWP zones (Javeed & Zameer, 2012). The reclassification of slope from poor (> 30 - steep) to very good GWP area (0–2 -flat) ranks from 5-1.

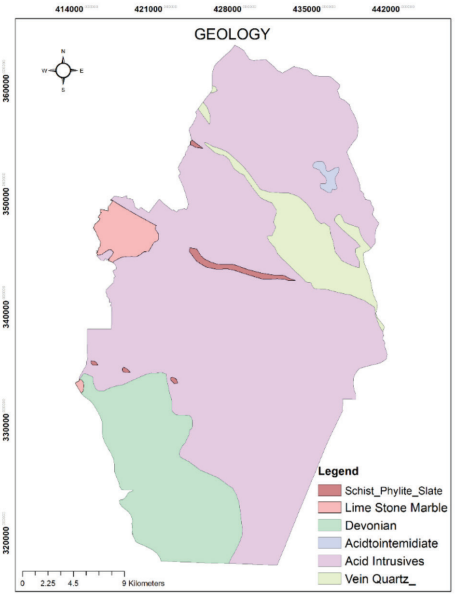

Figure 4: Geology unit

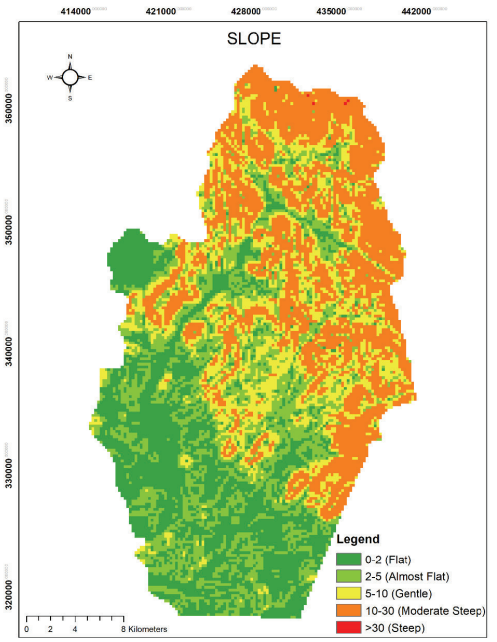

Figure 5: Slope

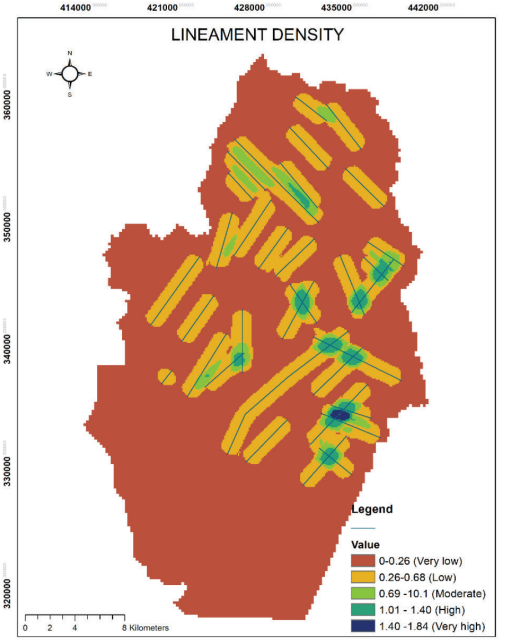

Figure 6: Lineament density

Lineament Density

Figure 6 depicts the classification of lineament density in km^2 units which are categorised into five (5) criteria: 0–0.26 (very low), 0.26–0.68 (low), 0.68–1.01 (moderate), 1.01–1.40 (high), and 1.40–1.84 (very high). The northeast area has high lineament density, while the south-central area has low lineament density. According to the reclassification of Lineament Density, which ranks from poor (1) to the most influential (5), most of the study area is covered by very low lineament density. Approximately only 0.1% of the study area is covered by very high lineament density (1.40–1.84).

Drainage Density

Figure 7 indicates the result of drainage density that has been classified into five (5) classes: 0–0.5 km^2 (very low), 0.5–1 km^2 (low), 1–1.5 km^2 (medium), 1.5–2 km^2 (high), > 2 km^2 (very high) The density drainage then reclassified according to the potential of groundwater area from very low (1) to very high (5). It is found that very high- and high-density areas are scattered almost at the centre of the study area. Meanwhile, the low drainage density covers

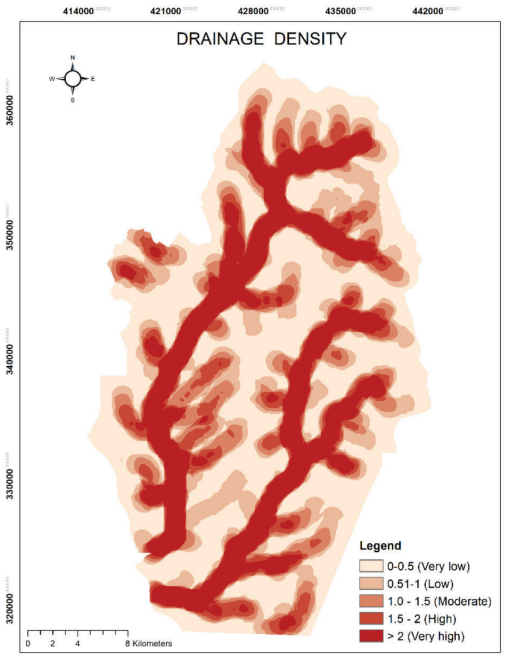

Figure 7: Drainage density

the edges of the study region. From these findings, it can be concluded that the centre of the study area with high drainage density has a high potential for GWP (Hussein *et al.,* 2017; Nigussie *et al.,* 2019).

Rainfall

As illustrated in Figure 8, the map of Mean Rainfall is divided into five categories: 174.74 mm–179.79 mm (very light), 179.9 mm–184.84 mm (light), 184.85 mm–189.89 mm (moderate), 189.89 mm–194.94 mm (heavy), and 194.95 mm–199.99 mm (very heavy). Based on the interpolation of mean monthly rainfall indicated, heavy and very heavy rainfall cover the northern part of the study area. These areas are considered very good GWP areas as high amounts of rainfall contribute to the high groundwater content (Manap, 2011). Meanwhile, moderate and light amount of rainfall occurs at the centre and the west part of Hulu Langat, respectively. The southern part of the study region experiences very light rainfall.

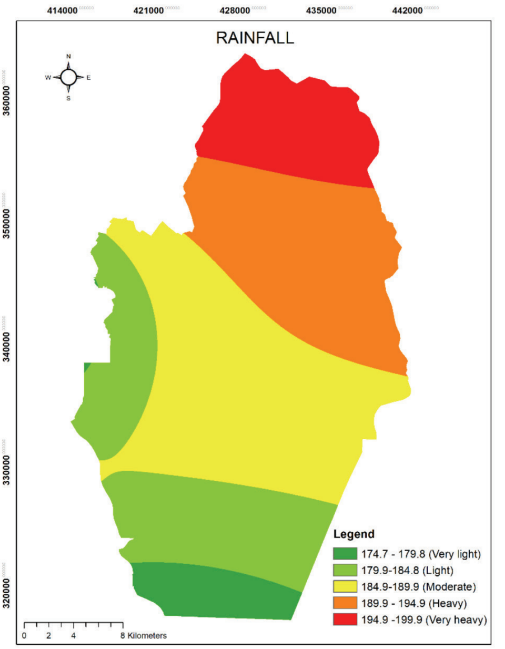

Figure 8: Rainfall

Elevation

Figure 9 shows 5 classifications of elevation which are -41.14-142.15 (very low), 142.16-314.33 (low), 314.34-525.39 (moderate), 525.4-808.66 (high), and > 808.67 (very high). The classification of groundwater potential area is based on the elevation from very low (1) to very high (5). The southwest area, which covers the area of low elevation, has a very high GWP area since water tends to accumulate in lower topographies compared to higher terrain (Adeyeye *et al.*, 2019). At the same time, the northern area is covered by high and very high elevations.

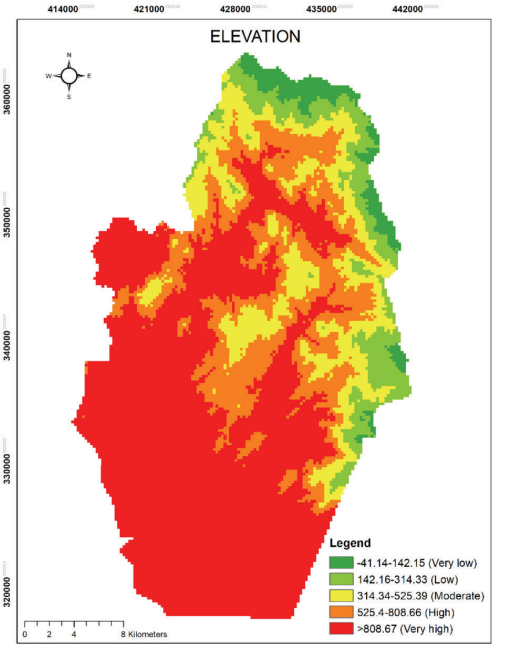

Figure 9: Elevation

Curvature

Figure 10 indicates the five (5) curvature classifications, which are -0.71 to -0.21 (very low), -0.2 to -0.07 (low), -0.06 to 0.06 (moderate), 0.07 to 0.23 (high), and 0.24 to 0.76 (very high). The analysis indicates that approximately 50% of the examined territory possesses a moderate groundwater potential, mainly concentrated in the southwestern area. The northern region is characterised by a prevalence of very low and very high curvatures.

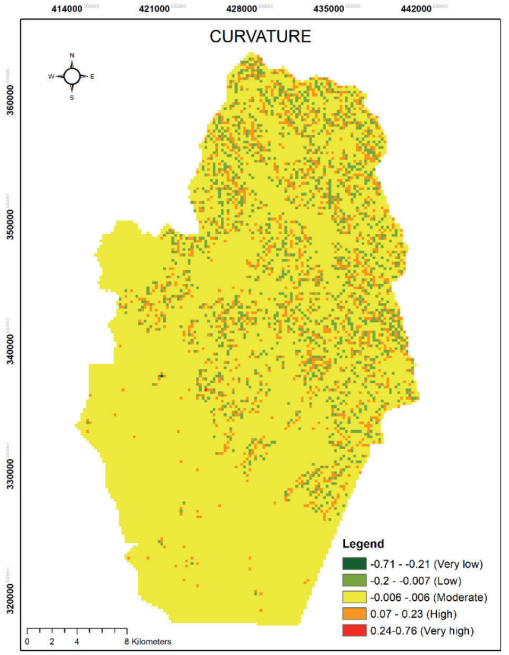

Figure 10: Curvature

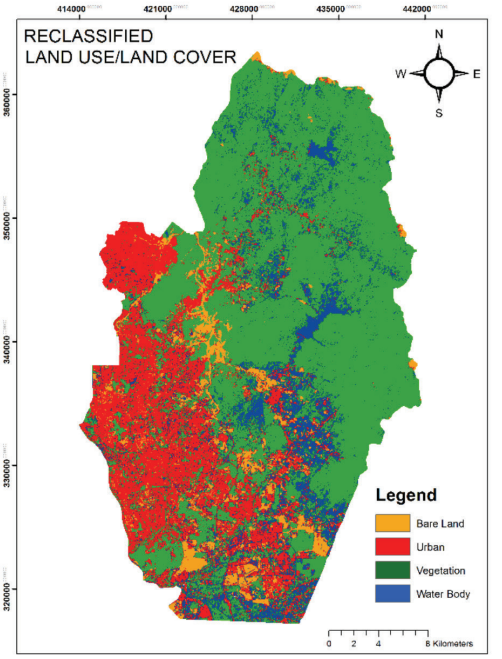

Figure 11: LULC

Land use/Land cover (LULC)

Land use/Land cover provides a high correlation with groundwater occurrence. Figure 11 shows the land cover for the study area. Based on the results, the study area comprises four (4) distinct classes, namely bare land, urban, vegetation, and water bodies. The findings indicate that vegetation and water bodies cover almost 70% of the area, primarily concentrated in the northeast region of Hulu Langat, which is recognised as a high GWP zone. On the other hand, bare land and urban land use account for almost 30% of the area, which is estimated to have a low GWP impact (Manap *et al.,* 2013).

Weight of Thematic Layer

The importance of the thematic layer has been established by considering several previous researchers (Jhariya *et al.*, 2016; Ahmadi *et al.*, 2021; Rahman *et al.*, 2022). Table 3 lists the scale values and weights assigned to the different classes of various conditioning factors. Elevation are considered the most influence factor with a weightage of 23%, followed by geology with a weightage of 19%. Geomorphology can be considered as a dominant factor with a weightage of 14%, followed by soil moisture (13%), slope (11%), lineament density (6%), rainfall (5%), drainage density (4%), curvature (3%), and LULC (2%). A single layer represents each of the listed parameters. A GPM map has been created by spatially manipulating these layers.

Groundwater Potential (GWP) Area

Two (2) GWPA maps are generated from soil moisture content obtained from Sentinel 1A and Landsat 8. All the 10 reclassified thematic layers are used to determine the potential area of groundwater along with weightage assigned using weight overlay in ArcGIS. The groundwater potential areas are divided into 3 classes ranging from poor to excellent. Figure 12 (a) depicts the GWP potential area in Hulu Langat derived from Sentinel 1A soil moisture and other 9 parameters.

It is concluded that the areas with excellent GWP are in the centre and the west of the study area. Most of these areas are flat surfaces and covered by water bodies and vegetation

Table 3: Scale values and weights assigned to different classes for different parameters

No	Factor	Class	Rating	Weightage
1	Elevation	-41.14–142.15	5 (Very high)	23%
		142.16–314.33	4 (high)	
		314.34–525.39	3 (Medium)	
		525.4–808.66	2 (Low)	
		525.4–808.66	1 (Very low)	
2	Geology	Phyllite_schist_limestone/stone	5 (Very high)	19%
		Limestone marble	4 (high)	
		Schist_ phyllite_stone	3 (Medium)	
		Acidtointermidiate	2 (Low)	
		Instructive Acid	1 (Very low)	
3	Geomorphology	MHE	1	14%
		SP	2	
		IP	3	
4	Soil Moisture	0–0.2	1 (Very low)	13%
		0.2–0.4	2 (Low)	
		0.4–0.6	3 (Medium)	
		0.6–0.8	4 (high)	
		0.6–0.8	5 (Very high)	
5	Slope	0–2	5 (Very high)	11%
		2–5	4 (high)	
		5–10	3 (Medium)	
		10–30	2 (Low)	
		> 30	1 (Very low)	
6	Lineament Density	0–0.26	1 (Very low)	6%
		0.26–0.68	2 (Low)	
		0.68–1.01	3 (Medium)	
		1.01–1.40	4 (high)	
		1.40–1.84	5 (Very high)	
7	Rainfall	174.7–179.8	1 (Very low)	5%
		179.8–184.8	2 (Low)	
		184.9–189.9	3 (Medium)	
		189.9–194.9	4 (high)	
		194.9–200	5 (Very high)	
8	Drainage Density	0–0.5	5 (Very high)	4%
		0.5–1.0	4 (high)	
		1.0–1.5	3 (Medium)	
		1.5–2.0	2 (Low)	
		> 2.0	1 (Very low)	
9	Curvature	-0.71 – -0.21	11 (Very low)	3%
		0.21– -0.07	2 (Low)	
		-0.07–0.06	3 (Medium)	
		0.06–0.23	4 (high)	
		0.24–0.76	5 (Very high)	
10	LULC	Bare Land	1	2%
		Urban	2	
		Vegetation	3	
		Water Body	4	

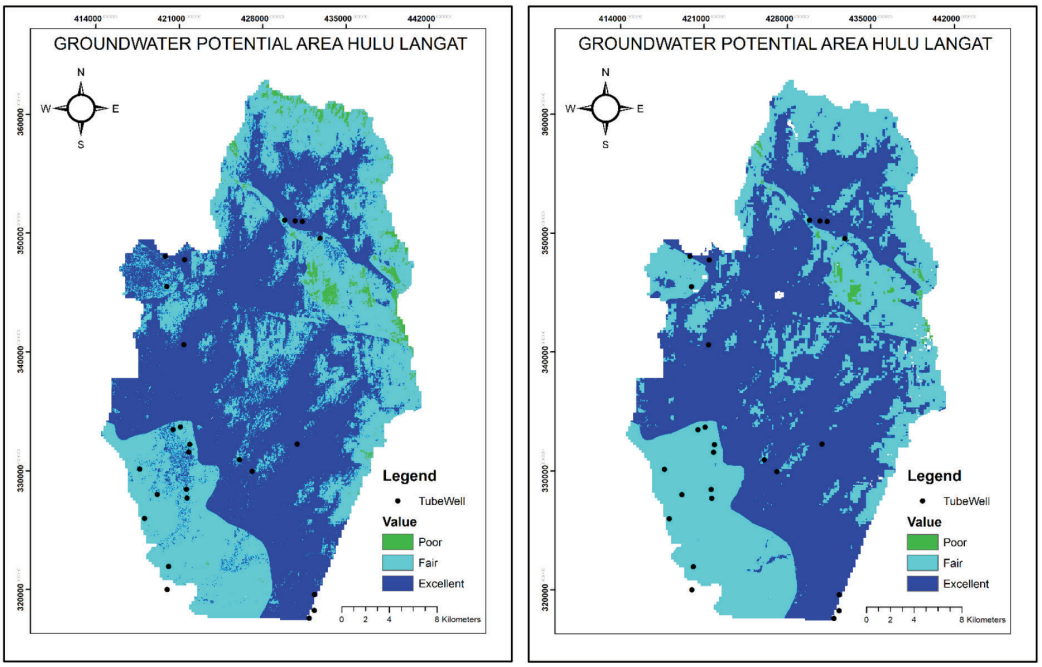

area, which contribute to infiltrations of water content (Hammouri *et al.,* 2012). The northern and eastern regions of the study areas are considered fair GWP areas as these areas contain nearly flat to steep slopes. Several areas in the northern region of Hulu Langat have poor GWP, resulting from high elevation with slopes greater than 30°.

As depicted in Figure 12 (b), the excellent GWP area generated from Landsat 8 soil moisture and other 9 parameters covers the centre of the study area. This area is characterised by low-elevation topography and flat terrain, as well as covered by vegetation and water bodies. The southern region of Hulu Langat is covered by fair GWP areas, consisting of high-elevation topographic regions. However, the western and northeastern parts of Hulu Langat are characterised by poor GWP areas. These regions are marked by moderate elevations, schist geological units, and steep slopes, which lead to lower GWP levels.

Table 4 shows the areas of GWP coverage for three (3) classes, including poor, fair, and excellent in the Hulu Langat region. The result from Sentinel 1A images shows that

Table 4: Groundwater potential area classes area

		Sentinel 1A Soil Moisture		**Landsat 8 Soil Moisture**		
No.	GWPA Classes	Area (km^2)	Percentage (%)	Area (km^2)	Percentage (%)	Difference (km^2)
1	Poor	13	1.6	4	0.50	±9
2	Fair	364	45.8	341	43.0	±23
3	Excellent	418	52.6	448	56.5	±30

approximately 52.3% of the study area has excellent GWP, compared to the result from Landsat 8 images which indicates 56.5% of the study area has excellent GWP. Sentinel 1A and Landsat 8 show that 45.8% and 43.0% of the study area have fair GWP, followed by 1.6% and 0.5% of the study area have poor GWP, respectively.

The GWPA maps obtained from both satellites have been validated by overlaying the map with tube wells data. Table 5 shows the number of tube wells that overlap with GWP areas. Twenty-four (24) tube wells have been discovered over the Hulu Langat region. The final map of areas with groundwater potential has been verified based on the distribution of tube wells. Out of 24 validation points, a total of 21 tube wells were located in fair and excellent GWP classes. The validation process indicates that the accuracy of groundwater potential area prediction for both Sentinel 1A and Landsat satellites is 85.71%. These results demonstrate a strong agreement between the predicted GWPA maps from both satellites and the actual groundwater regions identified from tube well data.

The correlation coefficients are computed to determine the optimum sensor for assessing soil moisture content. Figure 13 (a) shows the regression result of groundwater validation between the GWP area extracted from Sentinel 1A SAR and the tube well tunnel map. A total of eight (8) tube wells are located in the fair GWP area, while thirteen (13) tube wells are located in the excellent GWP area. The r value between GPWA retrieved from Sentinel 1A and the tube well map is 0.9826, which indicates a high correlation between both data.

Table 5: Data validation

Number of Tube wells Overlay with GWP classes area		
	Sentinel 1A	**Landsat 8**
GWP Classes		
Poor	0	0
Fair	8	13
Excellent	13	8
Total	21	21
Accuracy	**85.71%**	**85.71%**

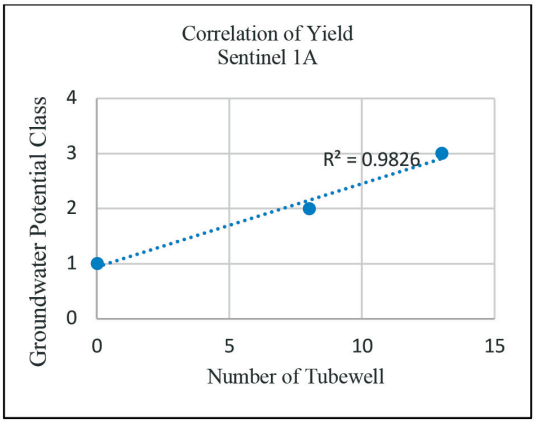

Figure 13: (a) Regression of yield Sentinel A

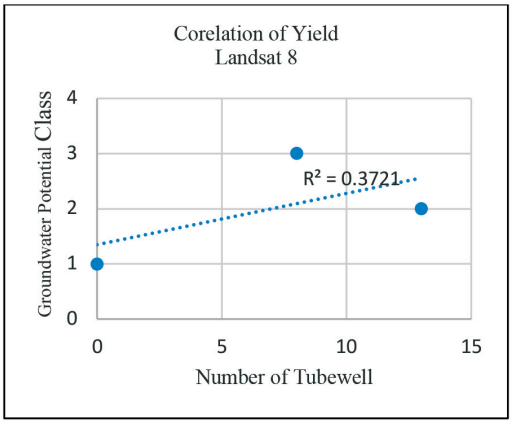

(b) Regression of yield Landsat 8

Figure 13 (b) reflects the regression result of groundwater validation between the GWP area extracted from Landsat 8 and the tube well map. There is no tube well located in a poor GWP area, 13 tube wells are located at fair GWP area, and 8 tube wells are located in a excellent GWP area. The r value between GPWA retrieved from Landsat 8 and the tube well map is 0.3721, which indicates a low correlation between both data. Thus, it can be concluded that Sentinel 1A is a better sensor for estimating the soil moisture content for GWP identification (Sutariya *et al.*, 2021).

Conclusion

This study offers a comprehensive insight into an integrated approach that combines satellite images and ground-based hydrological data to estimate the GWP area in Hulu Langat, Selangor. The accuracy of the findings is confirmed by validating them with the tube well of the study area. The soil moisture results from two different sensors effectively identify the GWP region in the study area. Sentinel 1A image yields 13% excellent GWP area, while Landsat 8 image soil extraction yields 8% excellent GWP area. The study concludes that GWP identification using Soil moisture extraction from the Sentinel 1A image is more effective, with a coefficient value of 0.98, compared to the Landsat 8 image, which has a coefficient value of 0.37. This underscores the significance of geospatial techniques in accurately determining the GWP area. The findings can benefit planners, policymakers, and local authorities in future project planning to ensure sustainable utilisation of groundwater resources.

Acknowledgements

This research was supported by Perkhidmatan Pembiayaan Yuran Penerbitan Artikel (PYPA), Universiti Teknologi MARA. We also thank our colleagues who provided insight and expertise that greatly assisted this research.

References

Abrams, W., Ghoneim, E., Shew, R., LaMaskin, T., Al-Bloushi, K., Hussein, S., AbuBakr, M., Al-Mulla, E., Al-Awar, M., & El-Baz, F. (2018). Delineation of groundwater potential (GWP) in the northern United Arab Emirates and Oman using geospatial technologies in conjunction with Simple Additive Weight (SAW), Analytical Hierarchy Process (AHP), and Probabilistic Frequency Ratio (PFR) techniques. *Journal of Arid Environments*, *157*, 77–96. https://doi.org/10.1016/j.jaridenv.2018.05.005

Adeyeye, O. A., Ikpokonte, E. A., & Arabi, S. A. (2019). GIS-based groundwater potential mapping within Dengi area, North Central Nigeria. *Egyptian Journal of Remote Sensing and Space Science*, *22*(2), 175–181. https://doi.org/10.1016/j.ejrs.2018.04.003

Alexakis, D. D., Mexis, F. D. K., Vozinaki, A. E. K., Daliakopoulos, I. N., & Tsanis, I. K. (2017). Soil moisture content estimation based on Sentinel-1 and auxiliary earth observation products. A hydrological approach. *Sensors* (Switzerland), *17*(6). https://doi.org/10.3390/s17061455

Chen, W., Li, H., Hou, E., Wang, S., Wang, G., Panahi, M., Li, T., Peng, T., Guo, C., Niu, C., Xiao, L., Wang, J., Xie, X., & Ahmad, B. (2018). GIS-based groundwater potential analysis using novel ensemble weights-of-evidence with logistic regression and functional tree models. *Science of the Total Environment*, *634*, 853–867. https://doi.org/10.1016/j.scitotenv.2018.04.055

Díaz-Alcaide, S., & Martínez-Santos, P. (2019). Review: Advances in groundwater potential mapping. *Hydrogeology Journal*, *27*(7), 2307–2324. https://doi.org/10.1007/s10040-019-02001-3

Elsheakh, D. N., & Abdallah, E. A. (2019). *Detection of underground water by using GPR*. www.intechopen.com

Entezari, M., Esmaeily, A., & Niazmardi, S. (2019). Estimation of soil moisture and

earth's surface temperature using landsat-8 satellite data. *International Archives of the Photogrammetry, Remote Sensing and Spatial Information Sciences - ISPRS Archives*, *42*(4/W18), 327–330. https://doi.org/10.5194/isprs-archives-XLII-4-W18-327-2019

Hammouri, N., El-Naqa, A., & Barakat, M. (2012). An integrated approach to groundwater exploration using remote sensing and geographic information system. *Journal of Water Resource and Protection*, *4*(9), 717–724. https://doi.org/10.4236/jwarp.2012.49081

Ibrahim-Bathis, K., & Ahmed, S. A. (2016a). Rainfall-runoff modelling of Doddahalla watershed—An application of HEC-HMS and SCN-CN in ungauged agricultural watershed. *Arabian Journal of Geosciences*, *9*(3), 1–16. https://doi.org/10.1007/s12517-015-2228-2

Ibrahim-Bathis, K., & Ahmed, S. A. (2016b). Geospatial technology for delineating groundwater potential zones in Doddahalla watershed of Chitradurga district, India. *Egyptian Journal of Remote Sensing and Space Science*, *19*(2), 223–234. https://doi.org/10.1016/j.ejrs.2016.06.002

Ifediegwu, S. I. (2022). Assessment of groundwater potential zones using GIS and AHP techniques: A case study of the Lafia district, Nasarawa State, Nigeria. *Applied Water Science*, *12*(1). https://doi.org/10.1007/s13201-021-01556-5

Javeed, A. R., & Zameer, A. R. A. (2020). Fuzzy logic-based GIS modeling for identification of ground water potential zones in the Jhagrabaria watershed of Allahabad District, Uttar Pradesh, India. *International Journal of Advances in Remote Sensing and GIS*, *1*(2), 218-233. https://www.researchgate.net/publication/347947284

Jhariya, D. C., Kumar, T., Gobinath, M., Diwan, P., & Kishore, N. (2016). Assessment of groundwater potential zone using remote sensing, GIS and multi criteria decision analysis techniques. *Journal Geological Society of India*, *88*(4), 481-492. http://dx.doi.org/10.1007/s12594-016-0511-9

Manap, M. A., Sulaiman, W. N. A., Ramli, M. F., Pradhan, B., & Surip, N. (2013). A knowledge-driven GIS modeling technique for groundwater potential mapping at the Upper Langat Basin, Malaysia. *Arabian Journal of Geosciences*, *6*(5), 1621–1637. https://doi.org/10.1007/s12517-011-0469-2

Misi, A., Gumindoga, W., & Hoko, Z. (2018). An assessment of groundwater potential and vulnerability in the upper Manyame Sub-Catchment of Zimbabwe. *Physics and Chemistry of the Earth*, *105*, 72–83. https://doi.org/10.1016/j.pce.2018.03.003

Mokadem, N., Redhaounia, B., Besser, H., Ayadi, Y., Khelifi, F., Hamad, A., Hamed, Y., & Bouri, S. (2018). Impact of climate change on groundwater and the extinction of ancient "Foggara" and springs systems in arid lands in North Africa: A case study in Gafsa basin (Central of Tunisia). *Euro-Mediterranean Journal for Environmental Integration*, *3*(1). https://doi.org/10.1007/s41207-018-0070-0

Mridha, G. C., Hossain, M. M., Uddin, M. S., & Masud, M. S. (2020). Study on availability of groundwater resources in Selangor state of Malaysia for an efficient planning and management of water resources. *Journal of Water and Climate Change*, *11*(4), 1050–1066. https://doi.org/10.2166/wcc.2019.043

Naghibi, S. A., Moghaddam, D. D., Kalantar, B., Pradhan, B., & Kisi, O. (2017). A comparative assessment of GIS-based data mining models and a novel ensemble model in groundwater well potential mapping. *Journal of Hydrology*, *548*, 471–483. https://doi.org/10.1016/j.jhydrol.2017.03.020

Nair, H. C., Padmalal, D., Joseph, A., & Vinod, P. G. (2017). Delineation of groundwater potential zones in river basins using geospatial tools—An example from Southern Western Ghats, Kerala, India.

Journal of Geovisualization and Spatial Analysis, *1*(1–2). https://doi.org/10.1007/s41651-017-0003-5

Nigussie, W., Hailu, B. T., & Azagegn, T. (2019). Mapping of groundwater potential zones using sentinel satellites (−1 SAR and -2A MSI) images and analytical hierarchy process in Ketar watershed, Main Ethiopian Rift. *Journal of African Earth Sciences*, *160*. https://doi.org/10.1016/j.jafrearsci.2019.103632

Nouri, H., & Faramarzi, M. B. (2017). Soil moisture estimation in rangelands using remote sensing (Case Study: Malayer, West of Iran). *Journal of Rangeland Science*, *7*(1). www.rangeland.ir

Osinowo, O. O., & Arowoogun, K. I. (2020). A multi-criteria decision analysis for groundwater potential evaluation in parts of Ibadan, southwestern Nigeria. *Applied Water Science*, *10*(11). https://doi.org/10.1007/s13201-020-01311-2

Parks, S., Byrnes, J., Abdelsalam, M. G., Laó Dávila, D. A., Atekwana, E. A., & Atya, M. A. (2017). Assessing groundwater accessibility in the Kharga Basin, Egypt: A remote sensing approach. *Journal of African Earth Sciences*, *136*, 272–281. https://doi.org/10.1016/j.jafrearsci.2016.11.002

Sajil Kumar, P. J., Elango, L., & Schneider, M. (2022). GIS and AHP based groundwater potential zones delineation in Chennai River Basin (CRB), India. *Sustainability* (Switzerland), *14*(3). https://doi.org/10.3390/su14031830

Saaty, T.L. (1990). *Decision making for leaders: The analytic hierarchy process for decisions in a complex world* (Vol. 2). Cologne, Germany: RWS Publications.

Serele, C., Pérez-Hoyos, A., & Kayitakire, F. (2020). Mapping of groundwater potential zones in the drought-prone areas of South Madagascar using geospatial techniques. *Geoscience Frontiers*, *11*(4), 1403–1413. https://doi.org/10.1016/j.gsf.2019.11.012

Sharma, P., Kumar, D., & Srivastava, H. S. (2018). Assessment of different methods for soil moisture estimation: A review. *Journal of Remote Sensing & GIS*, *9*(1), 57-73. https://www.researchgate.net/publication/325568808

ibanda, M., Dube, T., Seutloali, K., & Adelabu, S. (2015). Operational applications of remote sensing in groundwater mapping across sub-Saharan Africa. *Transactions of the Royal Society of South Africa*, *70*(2), 173–179. https://doi.org/10.1080/003591 9X.2015.1017024

Singh, S. K., Zeddies, M., Shankar, U., & Griffiths, G. A. (2019). Potential groundwater recharge zones within New Zealand. *Geoscience Frontiers*, *10*(3), 1065–1072. https://doi.org/10.1016/j.gsf.2018.05.018

SutarİYa, S., HİRapara, A., Meherbanalİ, M., Tİwarİ, M. k., Singh, V., & Kalubarme, M. (2021). Soil moisture estimation using Sentinel-1 SAR data and land surface temperature in Panchmahal District, Gujarat State. *International Journal of Environment and Geoinformatics*, *8*(1), 65–77. https://doi.org/10.30897/ijegeo.777434

Tajudin, N., Ya'acob, N., Ali, D. M., & Adnan, N. A. (2021). Soil moisture index estimation from Landsat 8 images for prediction and monitoring landslide occurrences in Ulu Kelang, Selangor, Malaysia. *International Journal of Electrical and Computer Engineering*, *11*(3), 2101–2108. https://doi.org/10.11591/ijece.v11i3.pp2101-2108

Wang, D., Xu, H., Shi, Y., Ding, Z., Deng, Z., Liu, Z., Xu, X., Lu, Z., Wang, G., Cheng, Z., & Zhao, X. (2021). The groundwater potential assessment system based on cloud computing: A case study in islands region. *Computer Communications*, *178*, 83–97. https://doi.org/10.1016/j.comcom.2021.06.028

Zamari, M. A., Musa, T. A., Mohamad, E. T., Musliman, I. A., & Aris, W. A. W. (2019). Geospatial approach for

groundwater exploration at UTM Johor Bahru campus. *International Archives of the Photogrammetry, Remote Sensing and Spatial Information Sciences - ISPRS Archives*, *42*(4/W16), 711–718. https://doi.org/10.5194/isprs-archives-XLII-4-W16-711-2019